Inline battery foil inspection using strobed Photometric Stereo

Christian Kapeller, Bernhard Blaschitz, and Ernst Bodenstorfer

AIT — Austrian Institute of Technology GmbH
High-Performance Vision Systems
Giefinggasse 4, 1210 Wien

Abstract Battery technology is a key component in current electric vehicle applications and an important building block for upcoming smart grid technologies. The performance of batteries depends largely on quality control in their production process. Defects introduced in the production of electrodes can lead to degraded performance and, more importantly, to short circuits that can cause accidents. In this contribution, we propose an inspection system that can detect defects, like missing coating, agglomerates, and pinholes on coated electrodes and acquire valuable production quality control metrics, like surface roughness. By employing Photometric Stereo (PS), a shape from shading algorithm, our system sidesteps difficulties that arise while optically inspecting the black to dark gray battery coating materials. We present in detail the acquisition concept of the proposed system, and analyze its acquisition-, as well as, its surface reconstruction performance. Further, we demonstrate the acquisition results of several common defect types that arise in foil production. Our system acquires at a production speed of 500 mm/s at a resolution of 50 µm per pixel resolution.

Keywords Optical inspection, inline inspection, high-speed, electrode, photometric stereo

DOI: 10.58895/ksp/1000124383-6 erschienen in:

Forum Bildverarbeitung 2020

DOI: 10.5445/KSP/1000124383 | https://www.ksp.kit.edu/site/books/m/10.58895/ksp/1000124383/

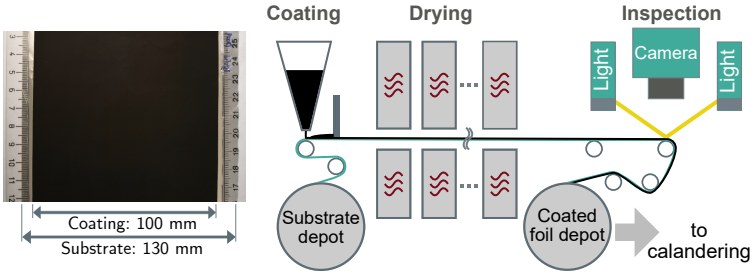

(a) NMC coated cathode (b) Inline coating process inspection

Figure 1.1: Illustration of a nickel manganese cobalt (NMC) cathode foil and the inline coating and inspection process.

1 Introduction

Battery technology is an important building block in the development of upcoming sustainable energy storage, energy distribution and electric mobility [1].

Electrode material is produced in the so-called coating process, in which electromechanically active material is applied onto a metal substrate foil.

A material comonly chosen for cathodes is nickel manganese cobalt (NMC) on aluminium substrate. Such cathodes exhibit a deep black texture, as shown in Fig. 6.1(a). A common choice for anodes is the dark gray colored graphite applied onto copper substrate.

For the coating process, illustrated in Fig. 6.1(b), a so-called *"slurry"*, a mixture of active material, binder material, condictive additives, and solvents, is prepared and placed into the application funnel. The slurry is applied onto the substrate with defined thickness. Following the doctor blade method [2] a blade mounted over the substrate lets slurry pass up a defined thickness. Next, the coated electrodes are dried and stored for the subsequent calandering process, where they are mechanically compressed. The goal of calandering is to improve electrode characteristics. Compression leads to more active material per volume, it homogenizes pore sizes, and reduces coating inhomogeneities. Finally, the calandered electrodes can be cut out and stacked on top of each other, interleaved with

insulating separator layers. The result can then be packaged into a final battery cell, for example in form of pouch- or prismatic cells.

An important factor influencing the electrical characteristics, and the safety of battery cells is the quality of the applied coating [3]. Ideally, the coating is finely grained and fully covers the substrate area evenly. However, especially when new kinds of coating mixes are developed, coating surfaces can deviate from this ideal conditions. A typical type of defect occurs, when the doctor blade gets clogged with agglomerates within the slurry mix, which leads to missing or unevenly applied coating behind the blade. The use of such defective electrodes in final cells degrades electrical capabilities, and, moreover, can lead to highly undesirable exothermic reactions causing harm to users [3]. Another process that can produce electrodes of suboptimal quality, is experimental battery research, when new kinds of slurry mixtures are tested. In the first case, optical quality assurance can help in ensuring that only cathodes of high quality are used for battery cells. In the second case, optical inspection can give valuable performance metrics about the quality of experimental slurry mixes.

In this work, we present an optical inspection system that can facilitate quality assurance in the coating process of anode and cathode foils that serve as building block for battery cells at production speeds of up to 500 mm/s at an optical lateral resolution of 50 µm/pix by means of photometric stereo surface reconstruction.

This paper is structured as follows. Section 2 provides an overview of existing systems for the inspection of battery foils. In Section 3 the proposed inspection system is described in detail. In Section 4 the proposed photometric stereo algorithms are explained in detail. Section 5 presents exemplary results of defects acquired with our system. Finally, Section 6 summarizes the content and provides an outlook to future work.

2 Related work

In the recent past, several optical battery foil inspection systems of various sensing modalities have been proposed. Just et al. [4] measure the infrared response of electrodes that are excited using elec-

tromagnetic radiation in order to detect applied silver particles. In contrast, our proposed system acquires material response in the visible frequency bands. Frommknecht et al. [5] combine a camera with ring-shaped illumination with a laser profilometer for defect detection. While the use of a laser profilometer allows for measuring absolute depth, its speed is limited to 500 Hz by the detectability of the laser line. Further, depth is measured only on a fraction of the foil area by the profilometer. Gruber et al. [6] employ hyper-spectral imaging and spectral ellipsometry to measure foil layer thickness while at the same time overcome specular reflections of the foil substrate. Our system, in contrast, reconstructs surfaces using a shape from shading approach.

3 Inline inspection using Photometric Stereo

In this section, we describe the proposed battery foil inspection system and its components in detail. Broadly, we can discern two subsystems, the sensor head ("Sensing & Acquisition") and the processing subsystem ("Processing & Control"), as schematically illustrated in Fig. 3.1. The sensor head is located within a coating machine and performs data acquisition and material illumination, while acquired data is processed on a PC situated in a back compartment of the machine outside of the, potentially toxic, atmosphere of the coating compartment.

3.1 Photometric Stereo acquisition and control

The sensing subsystem comprises (1) an FPGA-based controller hardware coordinating the acquisition, (2) a high-speed industrial camera, viewing at the material from top, (3) four line light sources illuminating the material from four directions, as well as, (4) a PC that coordinates image data acquisition and computes the foil surface representation.

According to Fig. 3.1, an FPGA-based controller ("Trigger Hardware"), an in-house development, ensures synchronization of material motion, control of lights, and camera acquisition. The trigger hardware translates 5 μm increments that are registered by a quadra-

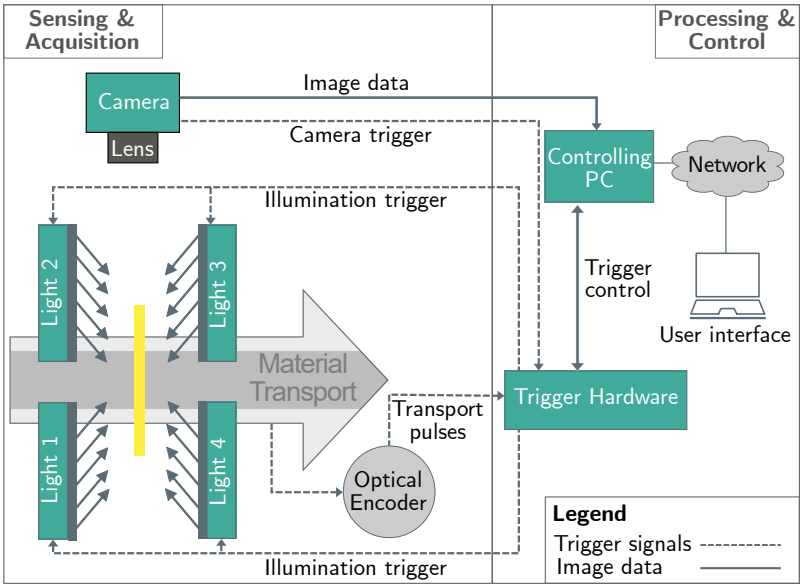

Figure 3.1: Schematic illustration of the system components. The sensing subsystem consists of a camera, viewing the electrode material from top, while it is illuminated in turn by four xposure:flash light sources for each increment measured by an optical encoder. A PC, shown in the right area, is used to setup acquisitions, and process the resulting image data, while acquisition timing is controlled by an FPGA based trigger hardware.

ture encoder to the system resolution of 50 µm increments per pixel. At each increment, the controller switches on one of the available four lights and triggers an image acquisition by the camera. This amounts to a frame trigger rate of 10 kHz at a material speed of 0.5 m/s. Fig. 6.3(a) shows the timing for switching the lights and triggering the camera. The frame period, i. e. the inverse of the frame trigger rate, corresponds to a material progress of 50 µm. Thus, as illustrated in Fig. 6.3(b), each object point (A, B, C, ...) is acquired four times under four different illumination directions.

As illumination, four xposure:flash [7] line light sources are located in a 4-orthogonal-configuration around the camera's field of view. Each light source contains a linear array of white high-power

LED's that allow fast strobing. The light sources are mounted at 45° rotation with respect to the transport direction, so to deliver high quality control data for defects that often occur in transport direction. They are mounted with a polar angle of 55°, as shown in Fig. 6.2(a). This angle was experimentally determined to be optimal for this type of material. We use four light sources due to the increased surface reconstruction stability [8] compared to the three lights required for determining three dimensional surface normal vectors. In order to have enough light for a proper signal, the light sources are strobed at a frequency of 10 kHz, which is only a small fraction of their maximum strobing frequency of 600 kHz. The irradiance in the object plane, generated by a single line light, is approximately 500.000 lx.

The camera, model Mikrotron eoSens 4CXP, is configured with a 12 mm lens to exhibit a field of view (FOV) of 116 mm in horizontal, and 200 μm in vertical direction. The FOV was chosen to acquire the whole width of the material and as well as the transition from substrate to the material. At 2336 pixels sensor width this amounts to an approximate resolution of 50 μm/px. The use of a multi-line acquisition regime enables observation of the same material positions illuminated by multiple light sources. As the material is continually moving, the obtained images are shifted by 0 to 3 pixels in transport direction for lights 1 to 4, for registration (see Fig. 6.3(b)).

As an AIT internal project we have constructed and successfully tested a system prototype in our laboratory. Fig. 3.2 shows construction drawings, as well as an image of the prototype system including a motorized roll simulation that allows us to thoroughly test system performance under various operating speeds.

3.2 Data processing

An industrial-grade PC is used for configuration of the acquisition subsystem and processing af acquired image data. Image data is acquired via the CoaxPress interface from the camera. Photometric Stereo results are processed, and stored to harddisk for further analysis. A graphical user interface is provided in order to enable an operator to review the results in real-time. As the PC is located within the machine, its user interface is remotely accessible via Ethernet-based networking.

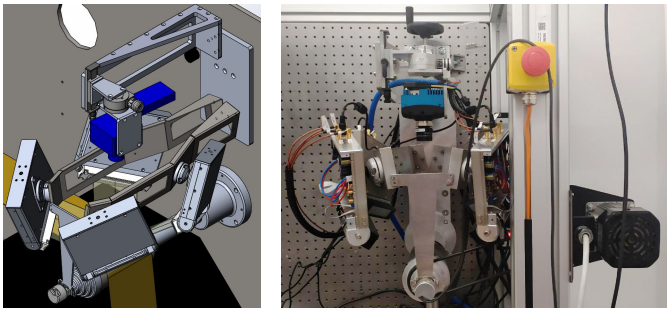

(a) Construction View (b) Machine simulation

Figure 3.2: System illustrations of (a) construction drawings, and (b) the system prototype with attached roll simulator operating in our laboratory environment. On top, the camera can be seen, while in middle area high-speed xposure:flash light sources are visible focusing on the roll in the lower region, which is driven by a motor on the right.

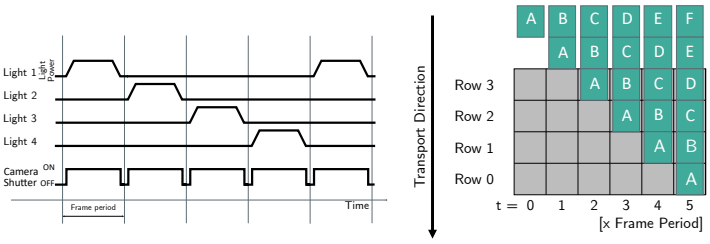

(a) Light and camera timing (b) Multi-line scanning

Figure 3.3: Illustration of the system's acquisition and light timing and System timing

4 Photometric Stereo Processing

The dark texture of the battery material, black for NMC coated cathodes to dark gray for anode foils, impedes direct optical intensity analysis. Either large amounts of light need to be used for illumination, which increases cost, or long camera exposure times need to be used, which limits the speed of the coating line. Further, 3D reconstructions can aid the quantitative assessment of electrode qual-

ity. For this reason, we analyze defects based on the reconstructed surface geometry of the material. To this end we perform surface reconstruction using Photometric Stereo [9], an shape-from shading algorithm, that is well suited for the observed diffuse material.

PS employs the Lambertian assumption of perfect diffuse material and infinitely distant, parallel light rays, and reconstructs surfaces based on observed light intensities of light reflected from surface points illuminated under several illumination angles. We compute surface normals and albedo from acquired image data that correspond to the four illumination directions using our PS algorithm [9]. In the following, we concisely summarize the method for the reader's convenience.

We determine surface normals $N_{i,j} \in \mathbb{R}^3$ and albedo $\rho_{i,j} \in \mathbb{R}$ on a discretely sampled domain of $M \times N$ pixels dimension, from n acquisitions $I_{i,j} \in \mathbb{R}^n$ illuminated by light sources of known direction $L \in \mathbb{R}^3$ relative to material surface. The matrix $M_{i,j} = \rho_{i,j} N_{i,j}$ represents surface normal vectors scaled by albedo at each location. From the known light directions $L = [X, Y, Z]$ with $X = [x_1, \ldots, x_n]$, $Y = [y_1, \ldots, y_n]$ and $Z = [z_1, \ldots, z_n]$, we construct a polynomial $P \in \mathbb{R}^{n \times 10}$ such that:

$$
\begin{aligned}
P &= [P_2, P_1, P_0], \text{with} \\
P_2 &= [X \odot X, Y \odot Y, Z \odot Z, X \odot Y, X \odot Z, Y \odot Z], \\
P_1 &= [X, Y, Z], \\
P_0 &= [1],
\end{aligned}
\tag{4.1}
$$

where $\odot$ represents the Hadamard product, P_2 denotes 2nd order basis functions, P_1 denotes surface normal vectors, and P_0 being a vector of length n modelling ambient illumination.

We determine surface normals, scaled by albedo $M_{i,j}$ using the following Tikhonov regularized model that can be solved using conjugate gradient descent.

$$
\min_{M_{i,j}} \frac{1}{2} \| P \cdot M_{i,j} - I_{i,j} \|^2 + \lambda \| \Gamma \cdot M_{i,j} \|^2 \tag{4.2}
$$

Here $\Gamma \in \mathbb{R}^{7 \times 10}$ denotes an identity matrix for $[P_2, P_0]$. A a scalar biasing parameter λ steers the model to be explained foremostly by the coefficients in P_1 containing the surface normal components.

By solving equation 4.2 we can retrieve surface normals and albedo from $M_{i,j}$ such that:

$$\rho_{i,j} = \sqrt{M_{i,j,1}^2 + M_{i,j,2}^2 + M_{i,j,3}^2} \tag{4.3}$$

$$N_{i,j} = \frac{M_{i,j}}{\rho_{i,j}} \tag{4.4}$$

Note, that in this application, we rely on regularization to successfully solve the model which is in principle underdetermined, using only four lights. We choose the regularized model because reconstructed surface normals are less prone to large scale surface pertubations [9]. Subsequently, we generate a depth map from surface normals N by normal integration using the the method of Frankot and Chellappa [10].

5 Experimental results

In this section, we present the qualitative results obtained by acquiring data of deliberately defective anode and cathode foils provided by researchers from AIT's on–premises coating pilot line facility. The samples have been specifically selected to provide a good overview of real-world defects that can occur in foil coating, such as missing coating, coating inhomogeneities, pinholes, agglomerations, cavities and cracks.

Our dataset comprises of two black colored nickel manganese cobalt (NMC) cathodes and two graphite anodes of dark gray texture. Coating was applied with a width of 100 mm onto substrates of approximately 130 mm width. The substrate's thickness is 20 µm, whereas, the applied coating thickness ranges from 30 to 450 µm. The samples were acquired at a speed of 500 mm/s. The results were obtained using the processing pipeline described in Section 4.

The most obvious type of defect is *missing coating*, as illustrated in Fig. 5.1 (a,b). In the present samples it is caused by agglomerates clogging the doctor blade and preventing new slurry to pass the blade in those regions. Sometimes these pollutions break free after a while, as can be seen in Fig. 5.1 (a). Electrodes with missing coating are unfit for use in cells. Large scale missing coating is obviously

visible in raw image data, small blade obliterations, however, may not reach down to the substrate material.

Such defects can be called *coating inhomogeneities*. An example can be seen in Fig. 5.1 (c). Coating inhomogeneities can cause, among others, degraded cell capacity [3], and can be mitigated to some extent by subsequent calandering. Inhomogeneities are hard to detect optically, especially on the black NMC material. They are, however, visible in surface normals and the derived depth map.

Pinholes are small diameter pores, depicted in Fig. 5.1 (c), are caused by small air bubbles bursting in the drying process and can reach down to the substrate. Pinholes can be caused by inadequate slurry mix, or drying parameters [3]. They are best visible in depth maps and invisible in raw image data. Note, that the shown sample additionally exhibits small dark spots that can, but don't always coincide with pinholes. Slurry containing large air bubbles can leave *cavities* or void areas, as shown in Fig. 5.1 (d). This sample further contains *cracks* in the coating area.

While all the previously discussed defects are variations of missing active material, *agglomerates* constitute of excess material, as shown in Fig.5.1 (d). Agglomerates can be caused by an incomplete slurry mix [3] and can potentially damage the calandering roll, or if not crushed there, pierce the separator foil in final cells.

Another observable coating property is the coating's *surface roughness*. Rough coating can damage the mechanical press in the calandering process following the coating step. Examples for low roughness is shown in Fig. 5.1 (a,b), while a sample of high roughness can be seen in Fig. 5.1 (c).

6 Conclusions and future work

In this paper we have presented an inline inspection system for battery foils that can acquire 2.5D images at speed of up to 500 mm/s with a lateral resolution of 50 µm/px. We achieve this performance using tight coupling of transport movement, interleaved strobing of four line lights and image acquistion using an FPGA-based controller. By employing Photometric Stereo surface reconstruction, our system is capable of visualizing fine surface details. After briefly

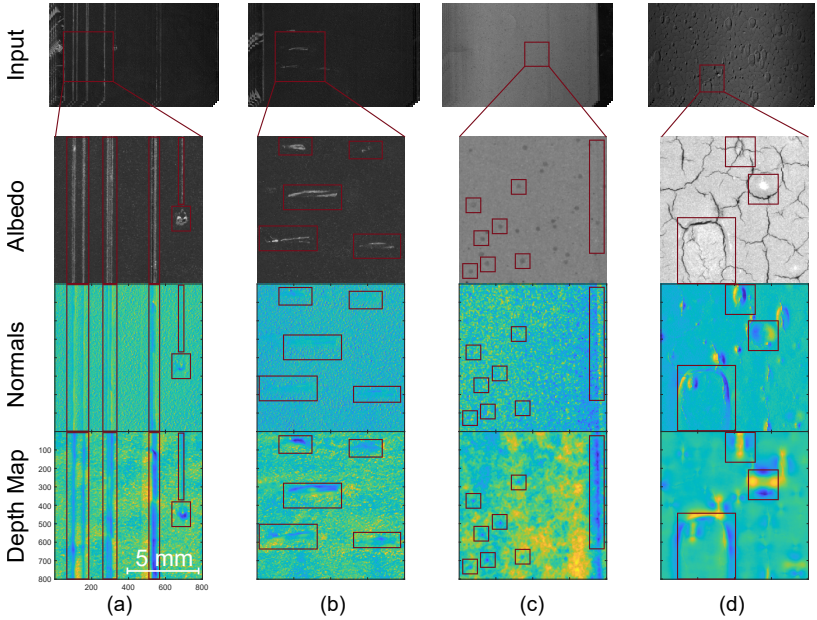

Figure 5.1: Coating defects occuring in two black NMC coated cathodes (a,b) and two dark gray graphite anodes (c,d). Defects are marked in red.

summarizing the state of the art, we have described the mechanical and optical sensing components in detail. Further, we have described our Photometric Stereo algorithm that is capable of visualizing fine surface details and defects in electrode material. Finally, we have presented qualitative results of several common foil defects in a foil data set obtained from an experimental battery production facility.

In the future, we will improve the system, so to achieve a speed of 2 m/s, while at the same time increasing the resolution to 10 µm/px, as part of the 3beliEVe project. Further, we will integrate machine-learning-based defect classification for electrodes into our system.

Acknowledgements

This work has received funding from the European Union's H2020 research and innovation program in the context of the 3beliEVe project under Grant Agreement no. 875033. Further, we would like to thank Katja Fröhlich, Lukas Neidhart and Andreas Gigl from AIT's center for Low Emission Transport for providing the electrode samples used in this work.

References

1. European Commission, "Europe on the move - Annex 2: Strategic Action Plan on Batteries," pp. 1–10, 2018.
2. H. Yang and P. Jiang, "Large-scale colloidal self-assembly by doctor blade coating," *Langmuir*, vol. 26, no. 16, pp. 13 173–13 182, 2010.
3. D. Mohanty, E. Hockaday, J. Li, D. K. Hensley, C. Daniel, and D. L. Wood, "Effect of electrode manufacturing defects on electrochemical performance of lithium-ion batteries: Cognizance of the battery failure sources," *Journal of Power Sources*, vol. 312, pp. 70–79, 2016.
4. P. Just, L. Ebert, T. Echelmeyer, and M. A. Roscher, "Infrared particle detection for battery electrode foils," *Infrared Physics and Technology*, vol. 61, pp. 254–258, 2013.
5. A. Frommknecht, M. Schmauder, L. Boonen, and C. Glanz, "Automated inline visual inspection and 3D measuring in electrode manufacturing," in *Optical Measurement Systems for Industrial Inspection XI*, no. June. SPIE, jun 2019, p. 66.
6. F. Gruber, P. Wollmann, B. Schumm, W. Grählert, and S. Kaskel, "Quality control of slot-die coated aluminum oxide layers for battery applications using hyperspectral imaging," *Journal of Imaging*, vol. 2, no. 2, pp. 1–11, 2016.
7. E. Bodenstorfer, "Ultra-schnell gepulste LED-Beleuchtung öffnet neue Dimension für optische Oberflächen-Inspektion," in *Talk: Scientific Vision Days 2018, Stuttgart; 05.11.2018 - 08.11.2018*, 2018.
8. O. Drbohlav and M. Chantler, "On optimal light configurations in photometric stereo," *IEEE International Conference on Computer Vision*, vol. II, pp. 1707–1712, 2005.

9. D. Antensteiner and S. Štolc, "Regularization in Higher-order Photometric Stereo Inspection for Non-Lambertian Reflections," in *Proc. International Joint Conference on Computer Vision, Imaging and Computer Graphics Theory and Applications*, 2020, pp. 253–259.
10. R. T. Frankot and R. Chellappa, "A Method for Enforcing Integrability in Shape from Shading Algorithms," *IEEE Transactions on Pattern Analysis and Machine Intelligence*, vol. 10, no. 4, pp. 439–451, 1988.